CTCF mediates the Activity-by-contact derived cis-regulatory hubs

Mick Lee[1,2*], Loïc Mangnier[3,4,5,6*], Cory C. Padilla[7], Dominic Paul Lee[1,2], Wilson Tan[1,2], Peter Yiqing Li [1,2], Wen Hao Zheng[1,2], Louis Gan[1,2], Ching Kit Chen[1,2,8,9], Yee Phong Lim[1,2,8,] Rina Miao Qin Wang[1,2,8], Steve Bilodeau[5,6,10,11], Alexandre Bureau[3,4,5], Roger Sik-Yin Foo[1,2#], Chukwuemeka George Anene-Nzelu[1,2,12,13#]

[1]Cardiovascular Disease Translational Research Programme, Yong Loo Lin School of Medicine, National University of Singapore, Singapore

[2]Genome Institute of Singapore, A*STAR, Singapore

[3]Centre de Recherche CERVO, Quebec City, Canada.

[4]Département de Médecine Sociale et Préventive, Université Laval, Quebec City, Canada.

[5]Centre de Recherche en données Massives de l'Université Laval, Québec, Québec, Canada, G1V 0A6.

[6]Centre de Recherche du Centre Hospitalier Universitaire de Québec – Université Laval, axe oncologie, Québec, Québec, Canada, G1R 3S3.

[7]Cantata Bio, 100 Enterprise Way Suite A-101 Scotts Valley, CA 95066

[8]Department of Paediatrics, Yong Loo Lin School of Medicine, National University of Singapore, Singapore

[9]Khoo Teck Puat-National University Children's Medical Institute, National University of Singapore, Singapore

[10]Centre de Recherche sur le Cancer de l'Université Laval, Québec, Québec, Canada, G1R 3S3.

[11]Département de Biologie Moléculaire, Biochimie Médicale et Pathologie, Faculté de Médecine, Université Laval, Québec, Québec, Canada, G1V 0A6.

[12]Montreal Heart Institute, Montreal, Quebec, Canada

[13]Department of Medicine, University of Montreal, Quebec, Canada

*These authors contributed equally

#Correspondence mdccgoa@nus.edu.sg, roger.foo@nus.edu.sg

ABSTRACT

The 3D chromatin architecture establishes a complex network of genes and regulatory elements necessary for transcriptomic regulation in development and disease. This network can be modeled by cis-regulatory hubs (CRH) which underscore the local functional interactions between enhancers and promoter regions and differ from other higher order chromatin structures such as topological associated domains (TAD). The Activity-by-contact (ABC) model of enhancer-promoter regulation has been recently used in the identification of these CRHs, but little is known about the role of CTCF on the ABC scores and the consequent impact on CRHs. Here we show that the loss of CTCF leads to a reorganization of the enhancer-promoter interactions resulting in a re-distribution of ABC scores of the putative enhancers in C57/bl6 mouse hearts. The loss of CTCF also leads to a global reduction of the total number of CRHs, and an increase in the size of the CRHs due to increase in the number of elements within each hub. In addition, CTCF loss led to more CRHs that cross TAD boundaries. These results provide another layer of evidence to support the importance of CTCF in the formation of regulatory networks necessary for gene regulation.

INTRODUCTION

The regulation of gene expression by the non-coding genome is an area of rapidly evolving research globally as it is implicated in different biological phenomena including organ development, cell-fate determination, tissue response to external stimuli and overall cellular homeostasis [1]. Furthermore, given the localization of the majority of disease-relevant genomic variations in non-coding regulatory regions [1], their involvement in disease pathogenesis is well documented. Accordingly, tremendous effort is deployed to annotate these regulatory elements in different species, tissues and cells [2-4]. To this end, different experimental protocols and computational algorithms have been applied to identify genome-wide regulatory elements responsible for controlling gene expression [5]. These include techniques such as ChIP-seq, ATAC-seq, DNase-seq, Hi-C, and functional genomics using CRISPR activation or inhibition studies etc., each with their strengths and limitations[5,6]. In addition, computational methods such the Activity by Contact (ABC) algorithm[3], TargetFinder, ELMER and others have been developed to integrate these datasets and identify gene-enhancer pairs. Similarly, large consortiums have been formed to annotate these regulatory elements in different tissues [7,8]. These studies provide a readily accessible resource and reference catalogue of the non-coding regulatory elements to the scientific community and help scientists unravel the role of regulatory regions in disease development and evaluate potential therapeutic strategies [9-11].

Besides the direct identification of enhancer-gene (E-G) pairs, other studies have demonstrated that enhancers and promoters often interact dynamically within a network often called cis-regulatory hubs (CRH), allowing for multiple regulatory connections [12,13]. These CRHs can be defined as 3D regulatory networks that constitute a complex organization of multi-loci connections of enhancers and promoters, connected in 3D space within the nucleus. They highlight direct and indirect contact between genes and distal regulatory elements and can help predict target genes for disease-relevant non-coding SNPs[13]. They are often bound by a cluster of transcription factors and have been implicated in gene co-regulation, lineage specification and disease development [12-14]. These hubs differ from other known 3D structures such as genomic compartments which constitute euchromatin or

heterochromatin regions. They also differ from TADs defined as units within which most enhancer-promoter interactions occur and loops which are pair-wise connections [15]. Identification of these CRHs is often done through detailed analysis of 3D contacts based on Hi-C data or using chromatin accessibility (ATAC or DNAse) to study co-accessible regions and thus construct these hubs [12,16-19]. A recent study proposed building these CRHs as a bipartite network using the Activity-by contact (ABC) algorithm [13]. The ABC algorithm combines ATAC-seq, ChiP-seq and Hi-C to rank the gene enhancers based on their regulatory impact and was shown to outperform other models such as HiChIP or TargetFinder in identifying regulatory enhancers [3,20]. Thus in addition to identifying and ranking enhancers, the ABC algorithm is used to generate a more predictive and physiologically relevant CRH[13], and these hubs were strongly enriched for disease-relevant genes and also helped explain disease heritability [13,21].

Given that the 3D genome architecture is a key component of the ABC algorithm, which is used to construct the CRHs, [13], it is of huge importance to understand the role of architectural proteins like CTCF. The CTCF protein often called the "genome weaver" plays a crucial function in the "folding" of the genome and bringing of enhancers into proximity to their distant target genes [15,22]. However, their role in regulating CRHs have not been explored. In this study, using mouse cardiomyocytes as a model of terminally differentiated non-dividing cells, we employ the ABC model to identify top cardiac gene-enhancers and then to study CRHs. We analyse the characteristics of CRHs containing tissue-specific genes, showing that these genes are enriched in multi-enhancer CRHs. We also show that in disease, there is a positive regulation of genes and enhancers within a CRH. Finally we show that loss of CTCF leads to a merging of CRHs and formation of new CRHs in the *Ctcf*-KO cells with resultant drastic change in the number and distribution of enhancers that cross the ABC threshold.

RESULTS

Cardiac Enhancer Landscape Identified Through Activity-By-Contact Algorithm

We performed ATAC-seq, H3K27ac ChiP-seq and HiChIP , to generate the ABC scores for the enhancer-gene pairs in the control adult mouse cardiomyocytes. Using an ABC cut-off of 0.01 [13], we identified 7000 out of 156,988 putative distal regulatory regions marked by H3K27ac

peaks and/or ATAC peak in the adult mouse CM that crossed the threshold. This represents about 5% of all putative regulatory regions predicted to have regulatory effect on their target genes and is similar to what was observed in another study [3]. With regards to the enhancer-gene (E-G) pairs, globally there were 34,496 E-G interactions with an average of 4.19 connections per gene, and 5.29 connections per enhancer in these control adult mouse CMs. Figure 1A shows examples of top-linked enhancers and their target genes for 2 cardiac disease-relevant genes *Mybpc3* and *Myh6*. The comprehensive list of ABC linked enhancers and target genes can be found in Supplementary Table 1. A literature search confirmed that at least 3 of the identified enhancers in our study have been validated. These include the *Nppa/Nppb* super enhancer located upstream of both genes and which has been shown to play a critical role in stress gene response of *Nppa/Nppb* during pressure-overload induced cardiac stress [23-25]. A separate enhancer for *Myh7* identified from the ABC scoring has also been validated previously in the mouse heart [26]. Deletion of this enhancer region led to downregulation of *Myh7* in mouse hearts[26]. Taken together, these previous studies provide support to the validity of our prediction model.

To provide further evidence that these ABC-linked enhancers regulate their putative target genes, we studied correlation between changes in gene expression versus changes in peak height of the ABC-linked enhancers during pressure overload-induced cardiac hypertrophy. Using RNA-seq and H3K27ac ChIP-seq datasets from mouse hearts subjected to transverse aortic constriction [23], we found that changes in gene expression correlates modestly with changes in H3K27ac peak signals (Pearson correlation= 0.34, $P < 2.2e\text{-}16$) (Fig 1B). The correlation was stronger when focussing only on genes and enhancers with greater or less than $\log_2$ 0.5 fold change after Transverse aortic constriction (Suppl Fig 1A) (Pearson correlation = 0.51, $P < 2.2e\text{-}16$). This result shows that globally, upon external stimuli, gene expression is regulated in the same direction as their ABC linked enhancers.

Loss Of CTCF Leads To Changes In The Enhancer Interactome And Changes In The ABC Scores Of Putative Enhancers

Next, to elucidate the role of CTCF in ABC scores and regulation of the CRHs, we also applied the ABC algorithm to the *Ctcf*-Knock out (*Ctcf*-KO) mouse cardiomyocytes. Given that previous publications have shown that the overall number of regulatory regions identified through

ChIP-seq or ATAC-seq after CTCF deletion remain mostly unchanged [27,28], with changes only observed in the peak heights, we focussed our attention on the HiChIP differences. We have previously published a genome-wide Hi-C in mouse cardiomyocytes [23]. A deeper analysis of the H3K27ac interactions through the first Micro-C/MNase mediated H3K27ac HiChIP in mouse CMs unravelled the enhancer interactome in the mouse heart. HiChIP presents advantages over Hi-C by providing better resolution with equal or lower sequencing depth [29] while the use of MNase in Micro-C provides better resolution for enhancer-promoter interactions compared to restriction-enzyme digest methods [30]. The H3K27ac HiChIP experiment was performed on two independent biological replicates each, and the data were merged to give a total of 160 million unique pairs for the *Ctcf*-KO and 126 million unique pairs for the control samples sufficient for HiChIP analysis[29]. For comparative analysis, the *Ctcf*-KO data was down sampled to 126M to match the control data. Using a window size of 10kb and an FDR of <0.1, we performed FitHiChIP [31] to identify the significant H3K27ac-anchored loops in our dataset. The results revealed 12,843 H3K27ac loops unique to control cells, 7,070 H3K27ac loops unique to *Ctcf*-KO cells and 483 shared H3K27ac loops between both conditions (Figure 2A, Supplementary Table 2). The KO-unique H3K27ac loops spanned longer distances than control-unique and shared H3K27ac loops (Figure 2B), consistent with previous studies using H3K4me3 HiChIP in zebrafish [27]. We further analysed these H3K27ac interaction anchors for the presence of CTCF using the Control CTCF ChIP-seq as reference. We discovered that 14% of these H3K27ac loop anchors occurred in regions with CTCF binding at both anchors in the control-unique group, while only 4.2% of the H3K27ac loops in the *Ctcf*-KO occurred in anchors with native CTCF binding. Concordantly, 56% of the H3K27ac loops had no native CTCF binding at the anchors in control, with the number increasing to 65% in the KO samples. The percentage of H3K27ac loops with native CTCF binding at one anchor was consistent at about 30% for both control and *Ctcf*-KO (Fig 2C). This shows that the loss of CTCF led to a 70% decrease in the H3K27ac loops that co-localize with CTCF at both anchors in the *Ctcf*-KO cells, with an increase in ectopic interactions between H3K27ac anchors without CTCF. Next we performed the aggregate peak analysis (APA) for the control and *Ctcf*-KO samples, the APA reveals enrichment for loop domains often bound by CTCF and Cohesin at the anchors [15]. Consistent with our previously published Hi-C data, and other studies that have performed aggregate analysis in different *Ctcf*-KO models [32], there was a marked decrease in the APA score from 3.33 in the control to 0.86 in the *Ctcf*-KO for all H3K27ac loops,

suggesting indeed the loss or weakening of loop domains in the *Ctcf*-KO samples [23].The APA score was also higher for the control unique and shared loops in the control samples, while the APA score for *Ctcf*-KO unique group was higher in the *Ctcf*-KO samples as anticipated, possible representing some re-arrangement of Cohesin in the *Ctcf*-KO group (Figure 2D)

We applied the ABC algorithm on the *Ctcf*-KO sample and observed that there were 36,226 regulatory elements that crossed the 0.01 threshold, resulting in 71,080 E-G interactions with similar number of expressed genes (~8,000) (Supplementary Table 1) in control and *Ctcf*-KO samples. This led to an increase in the average number of connections per gene to 8.14 in *Ctcf*-KO samples. Of the 71,080 enhancer-gene pairs only 20% (14,200 E-G pairs) were shared between control and Ctcf-KO. This increase in ABC scores could be due to increased interaction frequency and/or increased H3K27ac ChIP-seq upon CTCF loss. Interestingly we observed that the highest ranked ABC enhancer in the control had a score of 0.99, while the highest ranked enhancer in the *Ctcf*-KO sample had a score of 0.78 (scale of 0 – 1). Indeed the average score in the control was 0.054 while the average score in the *Ctcf*-KO was 0.028 (TTest P-value < 2.2e-16) . This suggests that the loss of CTCF led to gain of ectopic enhancers in the *Ctcf*-KO with a redistribution of the ABC scores of the enhancers.

Next we integrated the ABC results to generate the CRHs focussing first on the control samples. We identified 1,522 hubs in these control cardiomyocytes with about 70% of the hubs containing fewer than 5 elements (Fig 3A). Figure 3B shows 2 examples of such hubs containing cardiac genes: *Myom1* a gene involved in formation of myofibrils [33], and found in a simple hub while *Tnni3* a cardiac-specific sarcomeric gene is found in a more complex hub. Consistent with the correlation between gene expression and ABC-linked enhancers in heart disease, we also verified that genes and enhancers within the same hubs are positively correlated in same direction of change during cardiac stress, showing Pearson correlation of 0.32 (P <2.2e-16) (Figure 3C). This suggests a co-regulation of genes and enhancers found within the same hub upon external stimuli. We then ranked cardiac genes by FPKM and selected the top 50 genes, mostly cardiac-specific genes, to glean biological insights about the characteristics of CRHs that harbour these highly expressed genes. Our data revealed that highly expressed cardiac genes were more likely to be in hubs with more regulatory elements than non-highly expressed genes (Figure 3D). These cardiac-specific genes were also more likely to be found in hubs with higher number of promoters. Such multi-enhancer hubs has

been proposed as a mechanism to buffer against environmental stresses and genetic perturbations and thus provide phenotypic robustness to key genes [21,34]. On the other hand, hubs with high number of promoters are characteristic of lineage specific genes [13,21].

Loss Of CTCF Alters The Cis-Regulatory Hubs

Finally, we analysed the CRHs in the *Ctcf*-KO CMs and found a marked reduction in total number of CRHs from 1522 in control to 660 CRHs in the KO, accompanied with an increase in the number of elements per hub. Fig 4A shows example of the same hubs containing 2 cardiac genes shown in Fig 3A. Describe observation., Figure 4B shows the distribution of elements per hub, confirming a striking increase in the percentage of hubs with 10 or more elements. Associated with this increase in percentage of complex hubs, there was an increase in the average number of connections per gene in the *Ctcf*-KO cells, and a decrease in number of connections per enhancer (Fig 4C, Supplementary Fig 1B). We asked if this reduction in total number of CRHs was merely due to merging of CRHs or formation of new CRHs, and observed both cases. The merging of CRHs was observed primarily in the simple hubs (2-3 elements per hub) located within close proximity as 403 (82%) of 492 such simple hubs merged with 1 or more other hubs to form larger hubs. The proportion of the number of CRHs merging to form a new one varied, ranging from 2 merged CRHs to 15 merged CRHs Supplementary Fig 1C. For the larger hubs, there was mostly formation of new hubs, as genes gained new interaction and lost other interactions. To further confirm the importance of CTCF in the organization of these hubs, we compared CTCF binding sites in the control hubs vs *Ctcf*-KO hubs based on control CTCF ChIP-seq, and observed an enrichment of CTCF in the control hubs (fisher exact test odds ratio of 1.69, two sided $P < 2e\text{-}16$). Next, we analyzed the relationship between CRHs and TADs since TAD boundaries are enriched for CTCF [23], and earlier studies have shown that CRHs are generally constrained within TAD boundaries [13]. Indeed, using the TADs in the control as reference, our data showed that about 80% of CRHs in the control were contained within the same TAD while only 20% spanned more than 1 TAD. In contrast, about 45% of CRHs in KO were contained within a TAD while 50% of CRHs in the KO spanned more than 1 TAD (Fig 4D) while 5% were not within TAD boundaries, showing that the loss of CTCF leads to a reorganization of the CRHs with the formation of cross-TAD enhancer-promoter interactions.

DISCUSSION

Non-coding regulatory elements play crucial roles in development and disease and hold promise for next-generation therapeutic targets. While different studies by us and others have annotated these elements and CRHs in different cellular models, the role of CTCF in the ABC derived CRHs was yet to be studied. First, our study applied the ABC algorithm to the mouse heart, generating to the best of our knowledge, the first such ranked enhancer scores in mice hearts. Our findings confirm the positive correlation between genes and their ABC-linked enhancers in cardiac disease, and affirms that genes and enhancers within the same hub are co-regulated during pressure overload-induced cardiac hypertrophy. Integrating ABC to identify CRHs may thus represents another method to analyze for effect of regulatory SNPs on target genes, as the SNP may have effect on a target gene when they are in the same hub, even when there is no direct link through pair-wise enhancer-promoter analysis [13]. Analysis of the CRHs also suggests that tissue-specific genes are more likely to be contained in hubs with high connectivity and rich in distal elements. This increased number of E-P networks provides redundancy and phenotypic robustness while guaranteeing increased transcriptional activity thanks to the multi-enhancer networks.

Loss of CTCF affects the enhancer interactome, particularly impacting the H3K27ac interactions co-bound by CTCF. This leads to E-Ps that span larger distances and gain of new interactions. The loss of CTCF also leads to a re-organization of ABC-selected enhancers with a direct impact on the CRHs, resulting in fewer hubs but with more elements per hub. This implies a crucial role for CTCF in not only determining which enhancers cross the ABC threshold but also in the organization of the ABC-derived CRH. While this study focussed on the effect of loss of CTCF on overall CRH structure and its relationship with TAD boundaries, future studies will examine individual CRHs and their relationship to CTCF binding to ascertain how loss of CTCF can lead to local dysregulation of CRHs. Indeed, this finding has implications for mutations that affect local CTCF binding at regions that are not TAD boundaries, as it may lead to merging of 2 or more CRHs and thus the establishment of indirect connection between genes and enhancers within the newly formed hubs.

Our findings therefore demonstrate that CTCF plays a critical role in determining the membership of the CRHs as well as their organization, and thus plays a role in disease and cell type-specific gene expression through organization of these cis-regulatory hubs.

ABBREVIATIONS

ChIP-seq – Chromatin immunoprecipitation with sequencing

ATAC-seq – Assay for Transposase Accessible Chromatin with sequencing

Hi-C – High throughput chromatin conformation capture with sequencing

ABC – Activity by contact algorithm

DECLARATIONS

ETHICS APPROVAL: Animal protocol approved by the Institutional Animal Care and Use Committee (National University of Singapore)

CONSENT FOR PUBLICATION – The authors consent to publication of this article

AVAILABILITY OF DATA AND MATERIALS

The raw data supporting the conclusion of this article will be made available by the authors, without undue reservation.

COMPETING INTEREST

Cory C. Padilla works for Cantata Bio, developers of the HiChIP kit used in the study. The other authors declare that the research was conducted in the absence of any commercial or financial relationships that could be construed as a potential conflict of interest

FUNDING

This work was supported by grants from the National Medical Research Council (to Dr Foo), Start-up grants from the Montreal Heart Institute (Dr. Anene-Nzelu). The funding was used to purchase the reagents. Some data analyses were performed on computing resources from Compute Canada.

AUTHOR CONTRIBUTION

M.L, D.P.L, W.Z, L.G, C.C.K, Y.L, R.W, C.G.A.N performed the experiments, M.L, L.M, C.P, W.T, S.B, A.B, C.G.A.N provided data analysis. S.B, A.B, R.F, C.G.A.N Provided supervision for experiments and data analysis. All authors read and approved the manuscript

ACKNOWLEDGEMENTS

We thank Cantata Bio for providing the HiChIP kits

METHODS

Animal Experiments

Animal experiments were performed under a license approved by the Institutional Animal Care and Use Committee (National University of Singapore). *Ctcf*$^{flox/flox}$ mice harboring LoxP sites flanking exons 3 and 12 of the *Ctcf* gene against a C57/bl6 strain background were used as previously published [23]. Details of the source of the original strain has been documented in our earlier publication [23]. AAV9-cTnt-eGFP and AAV9-cTnt-Cre-tdTomato vectors encoding codon improved Cre recombinase or eGFP under the control of cardiac troponin T promoter were used for control and *Ctcf* knock-out respectively [23]. Experiments were performed on adult 6- to 8-week-old mice. 3 mice were used for each group, housed in 2 different cages. The numbers were based on our previously published study [23]. Cardiomyocytes were isolated from mouse hearts after 2 weeks of AAV9 injections for control and *Ctcf*-KO mice. CTCF knock-out was assessed by western blot, and upon confirmation, cells were used for subsequent experiments. Adeno-associated virus 9 (AAV9) virus for the delivery of Cre recombinase was generated as previously described [23]. For cardiomyocyte isolation, isoflurane anaesthesia is used before performing a thoracotomy to harvest the hearts as previously described [23].

H3k27ac HiChip Library Prep And Data Analysis.

Mouse adult cardiomyocytes were isolated following previously published protocol [23]. MNase-based HiChIP assay was performed on $2x10^6$ isolated CMs. Frozen cells were resuspended in 1× PBS and crosslinked with 3 mM DSG and 1% formaldehyde. Washed cells were digested with 0.75 µl MNase in 100 µl of nuclease digest buffer with $MgCl_2$. Cells were lysed with 1× RIPA, and clarified lysate was used for ChIP. H3K27ac antibody (Abcam 04729) was used to perform chromatin immunoprecipitation. The Protein A/G bead pulldown, proximity ligation, and libraries were prepared as described in the Dovetail protocol (Dovetail HiChIP MNase Kit). Libraries were sequenced on an Illumina Novaseq.

HiChIP paired-end reads were aligned with BWA MEM (version 0.7.17r1198-dirty) with the -5SP flag enabled with an index containing only the canonical chromosomes of the mm10 genome (available from the UCSC genome). The resulting alignments were then parsed with

pairtools (versions 0.3.0) with the following options --min-mapq 40 –walks-policy 5unque –max-inter-align gap 30 and the thre –chroms-path file corresponding to the size of the chromosomes used for the alignment index. Parse pairs were deduplicated, sorted with pairtools. Valid pairs were identified and through pairtools select (pair type = 'UU', 'UR', 'RU', 'uu', 'uU' and 'Uu') and downsampled to the lowest number of valid pairs in a sample (126 million in LACZ) with pairtools sample. Contact matrices in .hic format were generated with juicetools pre function (version 1.22.01).

FitHiChIP (version 9.1) was used to identify significant interactions ("loops") from the valid subsampled pairs at 10kb resolution with the following settings, loop type = all-to-all, coverage = bias correction, merge redundant loops = Yes, background model = FithHiChIP(L), FDR < 0.1, minimum interaction size =20kb, maximum interaction size = 2 mb. Conditionally unique (meaning only occurring in LACZ or CRE) and shared loops were identified with bedtools pairToPair (version 2.28.0) requiring both loop anchors to overlap the same coordinates be flagged as shared. Loop size was assessed by performing a two-sided Wilcoxson's rank-sum test on the distribution of loop ranges (distance between the two anchors). Loop anchors were then intersected the LACZ CTCF binding sites to determine the proportion of loops resulting from CTCF presence. P-values for CTCF mediated loops were obtained through a two-sided Fischer's Exact test. Aggregate Peak Analysis (APA) was computed with juicetools APA function. Loop anchors were used to as the sites to aggregate over at 10kb resolution. APA enrichment scores, loop center from the lower-left (LL) corner is shown as both an APA score (ratio of the mean of center to mean of LL) and a Z-score. APA normed output was used to plot the APA matrices.

H3K27ac HiChIP data were summarized and visualized with R, the package eulurr was used for the shared and unique loop Venn diagrams and ggplot2 for loop size and proportion of loops with CTCF binding site at the anchor. Additionally, ggplot2 was used to plot APA matrices with the geom_raster function, with the color scale set to the same min – max limits across all APA plots. At sites of interest, HiChIP loops files (in longrange format) were used to visualize loops along with ChIP-seq coverage and RNA-seq activity in the WashU Epigenome Browser (https://epigenomegateway.wustl.edu/).

Chip-Seq Experiment And Data Analysis

ChIP experiments on isolated CM were performed as described previously [23]. Briefly, CMs were cross-linked with 1% formaldehyde for 10 minutes at room temperature and quenched with glycine (0.125 mol/L final concentration). Cells were then washed in ice-cold PBS and pelleted and lysed in FA lysis buffer (10 mmol/L Tris-HCl, pH 8.0, 0.25% Triton X-100, 10 mmol/L EDTA, 0.1 mol/L NaCl). To facilitate cell lysis, the cell pellet was passed through a 27.5-gauge needle gently 20 times. Nuclei were pelleted by centrifugation resuspended in sonication buffer, and chromatin was fragmented via sonication to an average size of 200 to 300 bp (Bioruptor Plus, Diagenode). Chromatin was immunoprecipitated against H3K27ac (Abcam ab4729) or CTCF (EMD Millipore, catalog No. 07–729) overnight. Antibody-chromatin complexes were pulled down with Protein G Dynabeads (Invitrogen, catalog No. 10003D), washed with 0.1% SDS lysis buffer, and eluted with elution buffer (1% SDS, 10 mmol/L EDTA, 50 mmol/L Tris-HCl, pH 8). After cross-link reversal (4 hours of incubation at 65°C) and proteinase K treatment, immunoprecipitated DNA was extracted. ChIP DNA was quantified by fluorometric quantification (Thermo Fisher Scientific, Qubit dsDNA HS assay kit, catalog No. 32851). Library preparation was performed with the New England Biolabs Ultra II Kit according to the manufacturer's specifications and sequenced on the Illumina NextSeq High platform.

Paired-end reads were aligned to the mm10 genome using Bowtie2. The uniquely aligned reads were PCR-duplicate removed. Peak-calling was performed using Dfilter, and parameters were optimized for different antibodies. For H3K27ac, the parameters are: ks=60, lpval=6. For CTCF, ks=10, lpval=6, -nonzero, -refine. Reads were counted in 100-bp windows for each library and scaled to normalize for sequencing depth. Read counts in each window were then adjusted by normalizing their GCcontent against the average GC-content of all libraries. Peak height was obtained by summing the bin-wise normalized counts. Peak height was quantile-normalized to reduce technical variation. Supplementary Table 3 lists H3K27ac peaks in Sham and TAC treated mouse cardiomyocytes.

ATAC-Seq Experiment And Analysis

The ATAC-seq was performed according to previously published Omni-ATAC protocol [35] Briefly, 50,000 adult cardiomyocytes were pelleted at 500 g for 5 minutes. The cells were resuspended in 100 µl ATAC-resuspension buffer containing 0.5% NP40, 0.5 % Tween-20 and 0.01% Digitonin. The cells were left on ice for 5 minutes after which 1 ml of cold ATAC-RSB containing 0.1% Tween 20 was added to wash out the lysis buffer. The nuclei were pelleted at 500 g for 5 minutes, the supernatant was carefully removed and the nuclei were resuspended in 50 µl transposition mixture containing 25 µl of 2x TD buffer, 16.5 µl of PBS, 5 µl nuclease free water, 0.5 µl of 1% digitonin, 0.5 µl of 10% Tween-20 and 2.5 µl of transposase (Illumina Tagment DNA enzyme 1, Catalogue number 20034198). The reaction was incubated at 37°C for 30 minutes in a thermoshaker with 1000 RPM. After the reaction, DNA was extracted using the NEB Monarch® PCR & DNA cleanup kit (Catalogue number T1030L), PCR was performed using the Illumina/Nextera primers after which Ampure XP beads were used for library clean up. The resulting library was sequenced on Nextseq. Note that while ChIP-seq and HiChIP were performed on control and CTCF-KO cells, the ATAC-seq experiments were performed on a wild type C57/bl6 strain mice. ATACseq peaks were called on each sample using MACS2 (callpeak function with these parameters: -nomodel and -B). BedGraph files generated by MACS2 where normalized to read counts per million reads sequenced

ABC-Score And CRH Analysis

The ABC model defines active enhancers based on a quantitative score of DNAse, H3K27ac, and normalized Hi-C contact number[3]. This score is computed relative to a background activity over a 5-Mb window around a candidate element. Then, we set the threshold to 0.01; beyond which a candidate element is considered as a distal element. As an extension of the ABC-Score, CRHs were defined as bipartite networks between promoters and distal elements (igraph R package) [36] TADs were called using the directionality index as previously described. Pearson correlation analysis performed using R package

Figure 1:

A) USCS screenshot showing 2 examples of cardiac genes and their top ABC-linked enhancers

B) Pearson analysis showing correlation between differential expressed genes and differential enhancer peaks for ABC-linked enhancers during cardiac disease

Figure 2: H3K27ac HiChIP in Control and CTCF KO

A) Venn diagram showing number of FitHiChIP interactions in Control-unique and *Ctcf*-KO unique and shared loops
B) Box plot showing the loop sizes in the various groups. The loops in CTCF-unique interactions span longer distance than the interactions in Control unique CM
C) Bar chart showing distribution of CTCF at the FitHiChIP anchors. 14% of the loops have CTCF at both anchors in the control while only 4.2% of loops in the CTCF KO have CTCF on both anchors using the Control CTCF biding as reference
D) Aggregate Peak Analysis for the loops in Control and CTCF KO cells, showing a marked reduction of the APA and Z-score in the CTCF KO samples for all loops

Figure 3: CRH in control Cardiomyocytes

A) Bar chart showing distribution of number of elements per CRH
B) Examples of 2 CRHs containing cardiac genes *Myom1* and *Tnni3* in the control cardiomyocytes
C) Pearson correlation between differential expression of genes and enhancer peaks contained within the same CRHs during cardiac stress
D) Box plot showing characteristics of CRHs containing cardiac specific genes. These CRHs tend to have more enhancers and promoters

Figure 4: CRHs in the KO cells

A) Examples of 2 CRHs containing cardiac genes *Myom1* and *Tnni3* in the *Ctcf*-KO cardiomyocytes. Compared to the same CRHs in control, there is an increase in the number of elements in each hub
B) Bar chart showing distribution of elements per CRH in Control and *Ctcf*-KO. There is an increase in the percentage of CRHs with 10 or more elements from 15% in the Control to 60% in the CTCF KO cardiomyocytes

C) Bar chart showing number of connections per gene promoters and per enhancers. There is an increase in the average number of connections per gene in the *Ctcf*-KO CMs

D) Bar chart showing overlap of CRHs with TADs, 80% of TADs are contained in one TAD in the control while only 40% of CRHs are contained within one TAD in the CTCF KO. In contrast 20% of CRHs span 2 or more TADs in the control, while 50% of CRHs span 2 or more TADs in CTCF KO.

Supplementary figure 1

A) Pearson analysis showing correlation between differential expressed genes and differential enhancer peaks for ABC-linked enhancers during cardiac disease when taking into account only genes and enhancers with a fold change of log2 0.5

B) Bar chart showing number of connections per gene promoters and per enhancers in control and *Ctcf*-KO cells

C) Bar chart showing how many CRHs were merged to form a bigger CRH in *Ctcf*-KO cells, and the percentage of each category

1 Maurano, M. T. *et al.* Systematic localization of common disease-associated variation in regulatory DNA. *Science* **337**, 1190-1195, doi:10.1126/science.1222794 (2012).

2 Boix, C. A., James, B. T., Park, Y. P., Meuleman, W. & Kellis, M. Regulatory genomic circuitry of human disease loci by integrative epigenomics. *Nature* **590**, 300-307, doi:10.1038/s41586-020-03145-z (2021).

3 Fulco, C. P. *et al.* Activity-by-contact model of enhancer-promoter regulation from thousands of CRISPR perturbations. *Nat Genet* **51**, 1664-1669, doi:10.1038/s41588-019-0538-0 (2019).

4 Yao, L. *et al.* A comparison of experimental assays and analytical methods for genome-wide identification of active enhancers. *Nat Biotechnol*, doi:10.1038/s41587-022-01211-7 (2022).

5 Gasperini, M., Tome, J. M. & Shendure, J. Towards a comprehensive catalogue of validated and target-linked human enhancers. *Nat Rev Genet* **21**, 292-310, doi:10.1038/s41576-019-0209-0 (2020).

6 Anene-Nzelu, C. G., Lee, M. C. J., Tan, W. L. W., Dashi, A. & Foo, R. S. Y. Genomic enhancers in cardiac development and disease. *Nat Rev Cardiol*, doi:10.1038/s41569-021-00597-2 (2021).

7 Consortium, E. P. *et al.* Expanded encyclopaedias of DNA elements in the human and mouse genomes. *Nature* **583**, 699-710, doi:10.1038/s41586-020-2493-4 (2020).
8 Roadmap Epigenomics, C. *et al.* Integrative analysis of 111 reference human epigenomes. *Nature* **518**, 317-330, doi:10.1038/nature14248 (2015).
9 Alexanian, M. *et al.* A transcriptional switch governs fibroblast activation in heart disease. *Nature* **595**, 438-443, doi:10.1038/s41586-021-03674-1 (2021).
10 Frangoul, H. *et al.* CRISPR-Cas9 Gene Editing for Sickle Cell Disease and beta-Thalassemia. *N Engl J Med* **384**, 252-260, doi:10.1056/NEJMoa2031054 (2021).
11 Matharu, N. *et al.* CRISPR-mediated activation of a promoter or enhancer rescues obesity caused by haploinsufficiency. *Science* **363**, doi:10.1126/science.aau0629 (2019).
12 Espinola, S. M. *et al.* Cis-regulatory chromatin loops arise before TADs and gene activation, and are independent of cell fate during early Drosophila development. *Nat Genet* **53**, 477-486, doi:10.1038/s41588-021-00816-z (2021).
13 Mangnier, L., Joly-Beauparlant, C., Droit, A., Bilodeau, S. & Bureau, A. Cis-regulatory hubs: a new 3D model of complex disease genetics with an application to schizophrenia. *Life Sci Alliance* **5**, doi:10.26508/lsa.202101156 (2022).
14 Di Giammartino, D. C., Polyzos, A. & Apostolou, E. Transcription factors: building hubs in the 3D space. *Cell Cycle* **19**, 2395-2410, doi:10.1080/15384101.2020.1805238 (2020).
15 Rao, S. S. *et al.* A 3D map of the human genome at kilobase resolution reveals principles of chromatin looping. *Cell* **159**, 1665-1680, doi:10.1016/j.cell.2014.11.021 (2014).
16 Li, T., Jia, L., Cao, Y., Chen, Q. & Li, C. OCEAN-C: mapping hubs of open chromatin interactions across the genome reveals gene regulatory networks. *Genome Biol* **19**, 54, doi:10.1186/s13059-018-1430-4 (2018).
17 Madsen, J. G. S. *et al.* Highly interconnected enhancer communities control lineage-determining genes in human mesenchymal stem cells. *Nat Genet* **52**, 1227-1238, doi:10.1038/s41588-020-0709-z (2020).
18 Oudelaar, A. M. *et al.* A revised model for promoter competition based on multi-way chromatin interactions at the alpha-globin locus. *Nat Commun* **10**, 5412, doi:10.1038/s41467-019-13404-x (2019).
19 Pliner, H. A. *et al.* Cicero Predicts cis-Regulatory DNA Interactions from Single-Cell Chromatin Accessibility Data. *Mol Cell* **71**, 858-871 e858, doi:10.1016/j.molcel.2018.06.044 (2018).
20 Anene-Nzelu, C. G. *et al.* Assigning Distal Genomic Enhancers to Cardiac Disease-Causing Genes. *Circulation* **142**, 910-912, doi:10.1161/CIRCULATIONAHA.120.046040 (2020).
21 Tsai, A., Alves, M. R. & Crocker, J. Multi-enhancer transcriptional hubs confer phenotypic robustness. *Elife* **8**, doi:10.7554/eLife.45325 (2019).
22 Ong, C. T. & Corces, V. G. Enhancer function: new insights into the regulation of tissue-specific gene expression. *Nat Rev Genet* **12**, 283-293, doi:10.1038/nrg2957 (2011).
23 Lee, D. P. *et al.* Robust CTCF-Based Chromatin Architecture Underpins Epigenetic Changes in the Heart Failure Stress-Gene Response. *Circulation* **139**, 1937-1956, doi:10.1161/CIRCULATIONAHA.118.036726 (2019).

24 Man, J. C. K. *et al.* Genetic Dissection of a Super Enhancer Controlling the Nppa-Nppb Cluster in the Heart. *Circ Res* **128**, 115-129, doi:10.1161/CIRCRESAHA.120.317045 (2021).

25 Sergeeva, I. A. *et al.* Identification of a regulatory domain controlling the Nppa-Nppb gene cluster during heart development and stress. *Development* **143**, 2135-2146, doi:10.1242/dev.132019 (2016).

26 Dickel, D. E. *et al.* Genome-wide compendium and functional assessment of in vivo heart enhancers. *Nat Commun* **7**, 12923, doi:10.1038/ncomms12923 (2016).

27 Franke, M. *et al.* CTCF knockout in zebrafish induces alterations in regulatory landscapes and developmental gene expression. *Nat Commun* **12**, 5415, doi:10.1038/s41467-021-25604-5 (2021).

28 Kubo, N. *et al.* Promoter-proximal CTCF binding promotes distal enhancer-dependent gene activation. *Nat Struct Mol Biol* **28**, 152-161, doi:10.1038/s41594-020-00539-5 (2021).

29 Mumbach, M. R. *et al.* HiChIP: efficient and sensitive analysis of protein-directed genome architecture. *Nat Methods* **13**, 919-922, doi:10.1038/nmeth.3999 (2016).

30 Hsieh, T. S. *et al.* Resolving the 3D Landscape of Transcription-Linked Mammalian Chromatin Folding. *Mol Cell* **78**, 539-553 e538, doi:10.1016/j.molcel.2020.03.002 (2020).

31 Bhattacharyya, S., Chandra, V., Vijayanand, P. & Ay, F. Identification of significant chromatin contacts from HiChIP data by FitHiChIP. *Nat Commun* **10**, 4221, doi:10.1038/s41467-019-11950-y (2019).

32 Nora, E. P. *et al.* Targeted Degradation of CTCF Decouples Local Insulation of Chromosome Domains from Genomic Compartmentalization. *Cell* **169**, 930-944 e922, doi:10.1016/j.cell.2017.05.004 (2017).

33 Hang, C. *et al.* Knockout of MYOM1 in human cardiomyocytes leads to myocardial atrophy via impairing calcium homeostasis. *J Cell Mol Med* **25**, 1661-1676, doi:10.1111/jcmm.16268 (2021).

34 Osterwalder, M. *et al.* Enhancer redundancy provides phenotypic robustness in mammalian development. *Nature* **554**, 239-243, doi:10.1038/nature25461 (2018).

35 Corces, M. R. *et al.* An improved ATAC-seq protocol reduces background and enables interrogation of frozen tissues. *Nat Methods* **14**, 959-962, doi:10.1038/nmeth.4396 (2017).

36 Csardi G, N. T. The igraph software package for complex network research. *Int. J. Complex Syst.* (2006).

A

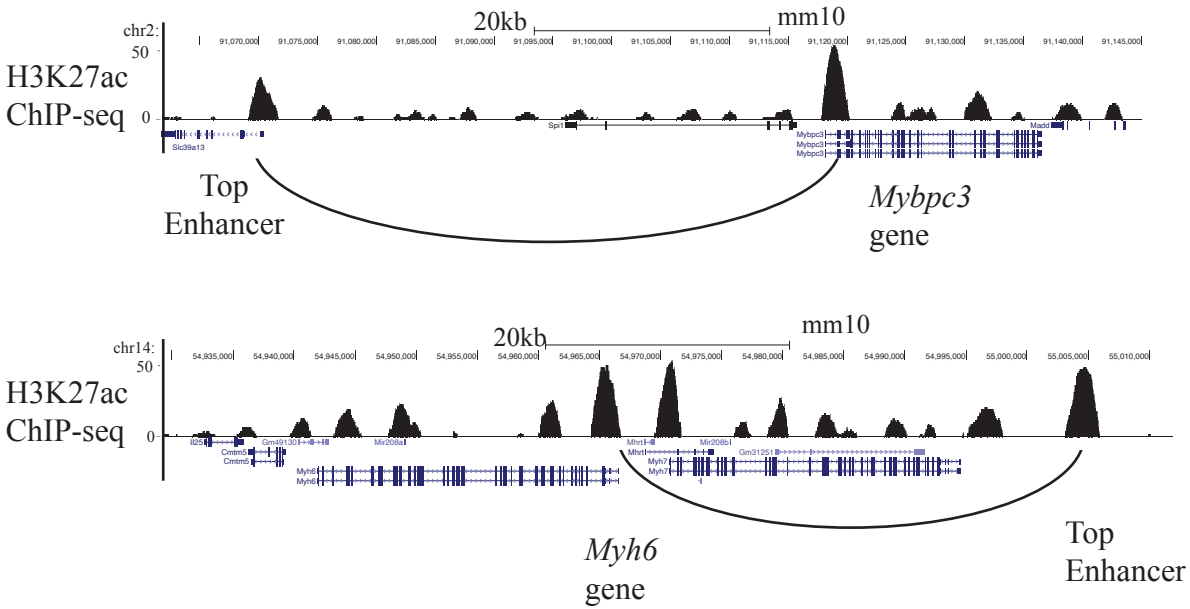
20kb
mm10
chr2:
50
0
H3K27ac
ChIP-seq
Top
Enhancer
Mybpc3
gene
20kb
mm10
chr14:
50
0
H3K27ac
ChIP-seq
Myh6
gene
Top
Enhancer

B

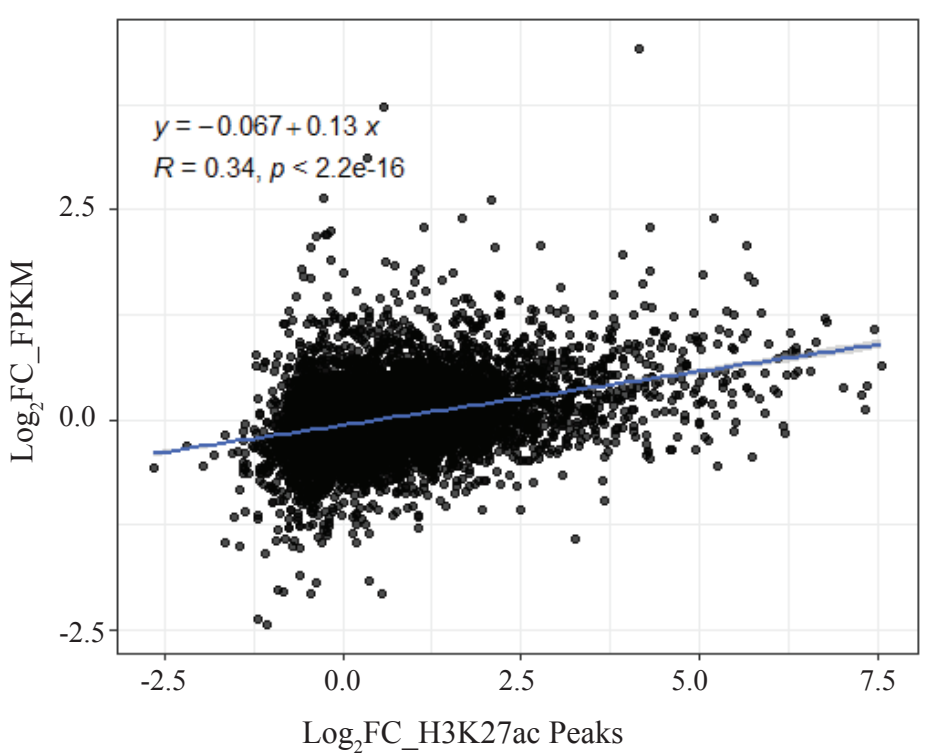
y = −0.067 + 0.13 x
R = 0.34, p < 2.2e-16
2.5
0.0
-2.5
Log2FC_FPKM
-2.5
0.0
2.5
5.0
7.5
Log2FC_H3K27ac Peaks

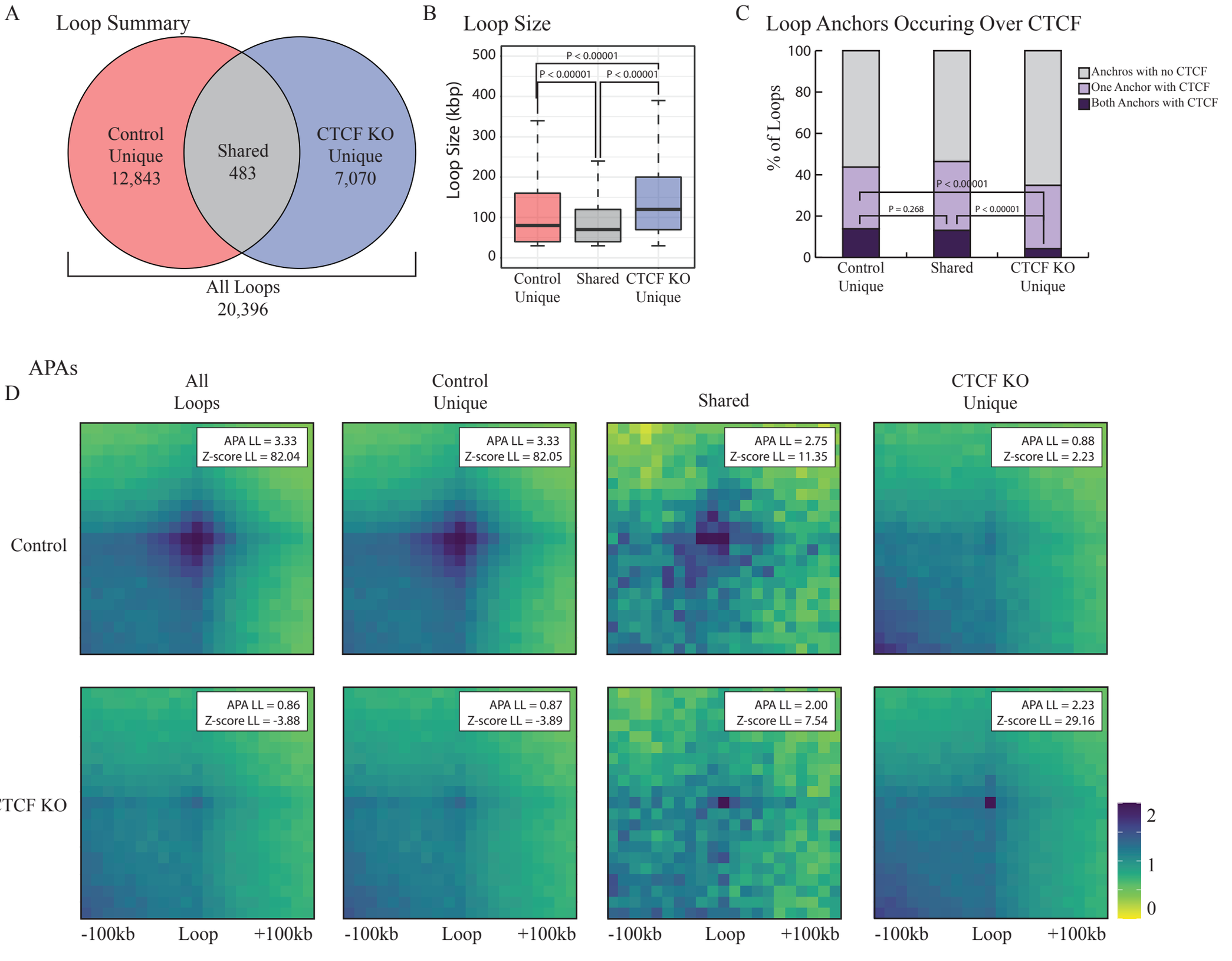
A
Loop Summary
Control Unique 12,843
Shared 483
CTCF KO Unique 7,070
All Loops 20,396
B
Loop Size
Loop Size (kbp)
P < 0.00001
P < 0.00001
P < 0.00001
Control Unique
Shared
CTCF KO Unique
C
Loop Anchors Occuring Over CTCF
% of Loops
Anchros with no CTCF
One Anchor with CTCF
Both Anchors with CTCF
P = 0.268
P < 0.00001
P < 0.00001
Control Unique
Shared
CTCF KO Unique
D
APAs
All Loops
Control Unique
Shared
CTCF KO Unique
Control
CTCF KO
APA LL = 3.33
Z-score LL = 82.04
APA LL = 3.33
Z-score LL = 82.05
APA LL = 2.75
Z-score LL = 11.35
APA LL = 0.88
Z-score LL = 2.23
APA LL = 0.86
Z-score LL = -3.88
APA LL = 0.87
Z-score LL = -3.89
APA LL = 2.00
Z-score LL = 7.54
APA LL = 2.23
Z-score LL = 29.16
-100kb
Loop
+100kb

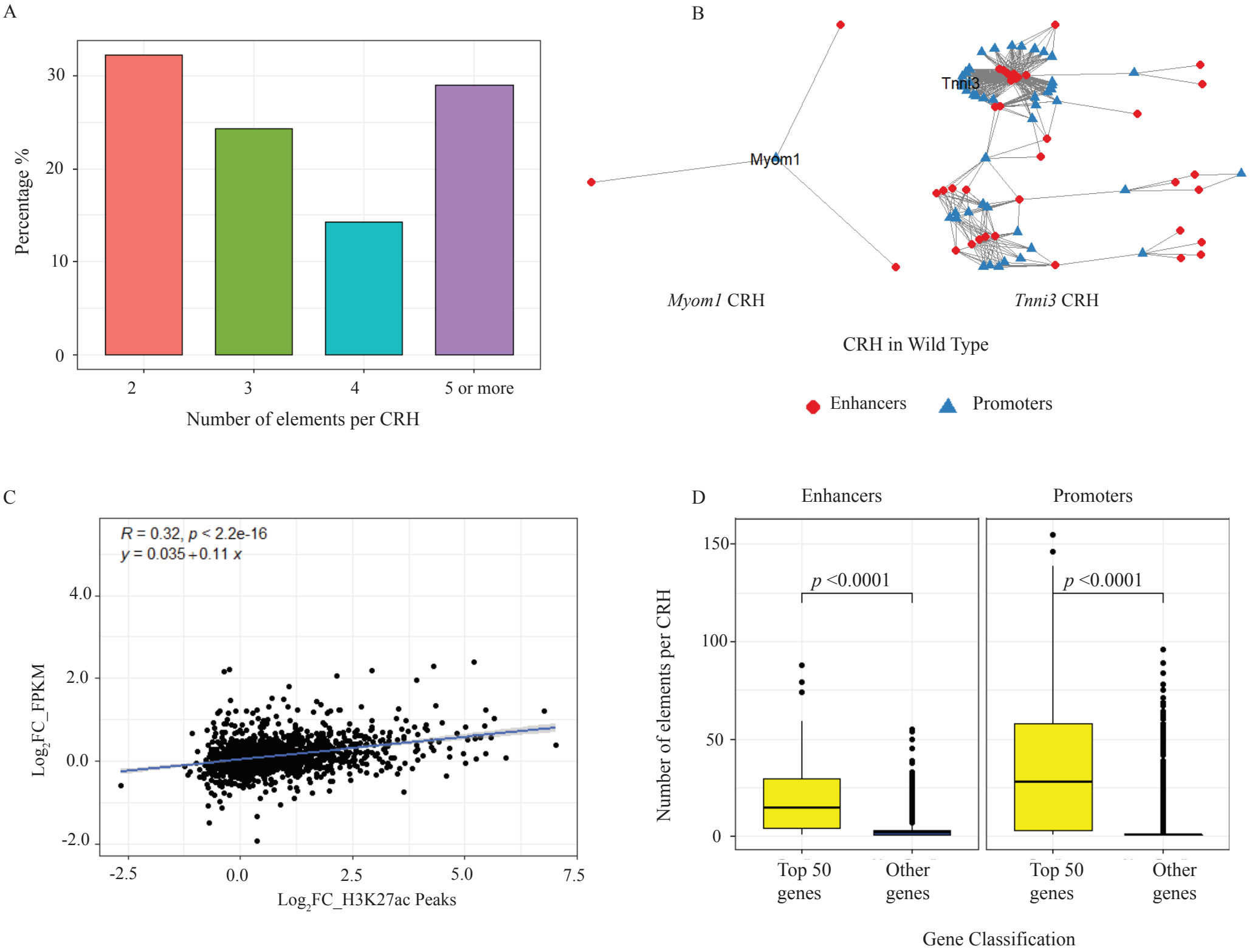
A
Percentage %
30
20
10
0
2
3
4
5 or more
Number of elements per CRH
B
Tnni3
Myom1
Myom1 CRH
Tnni3 CRH
CRH in Wild Type
Enhancers
Promoters
C
R = 0.32, p < 2.2e-16
y = 0.035 + 0.11 x
4.0
2.0
0.0
-2.0
Log2FC_FPKM
-2.5
0.0
2.5
5.0
7.5
Log2FC_H3K27ac Peaks
D
Enhancers
Promoters
150
100
50
0
Number of elements per CRH
p <0.0001
p <0.0001
Top 50 genes
Other genes
Top 50 genes
Other genes
Gene Classification

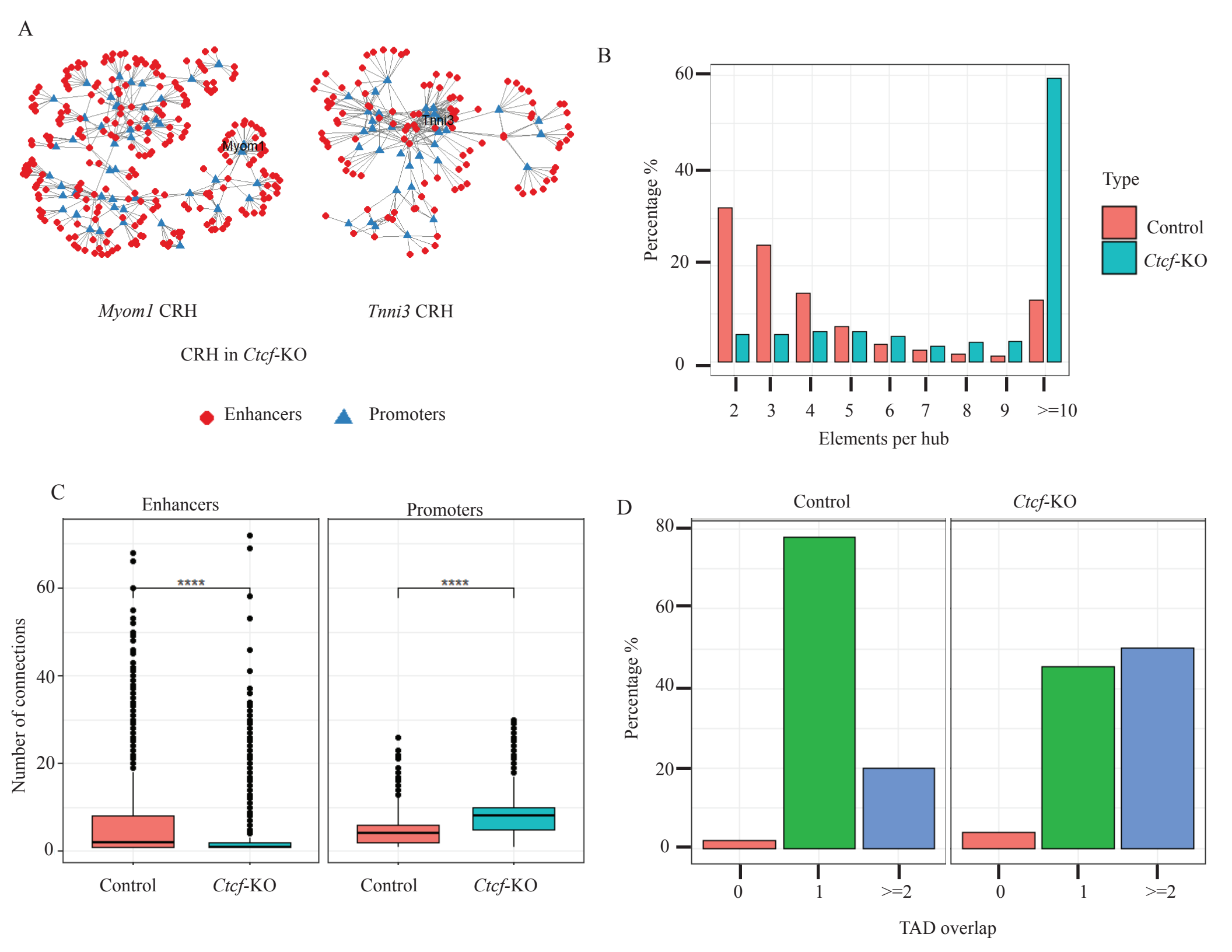
A
Myom1
Tnni3
Myom1 CRH
Tnni3 CRH
CRH in Ctcf-KO
Enhancers
Promoters
B
Percentage %
Elements per hub
Type
Control
Ctcf-KO
C
Enhancers
Promoters
Number of connections
****
Control
Ctcf-KO
D
Control
Ctcf-KO
Percentage %
TAD overlap

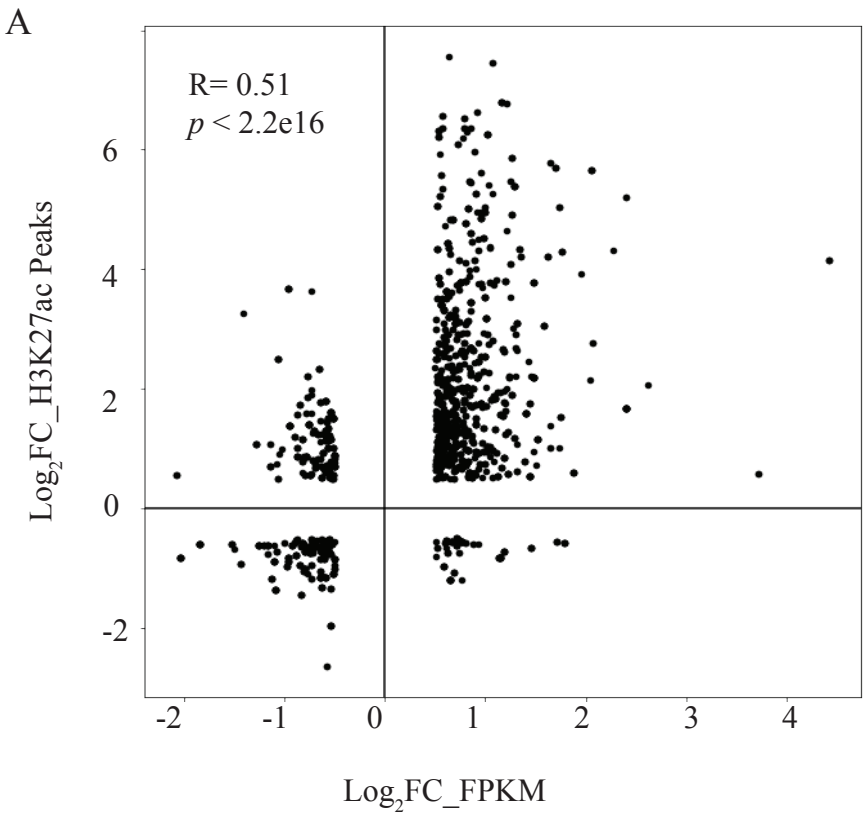

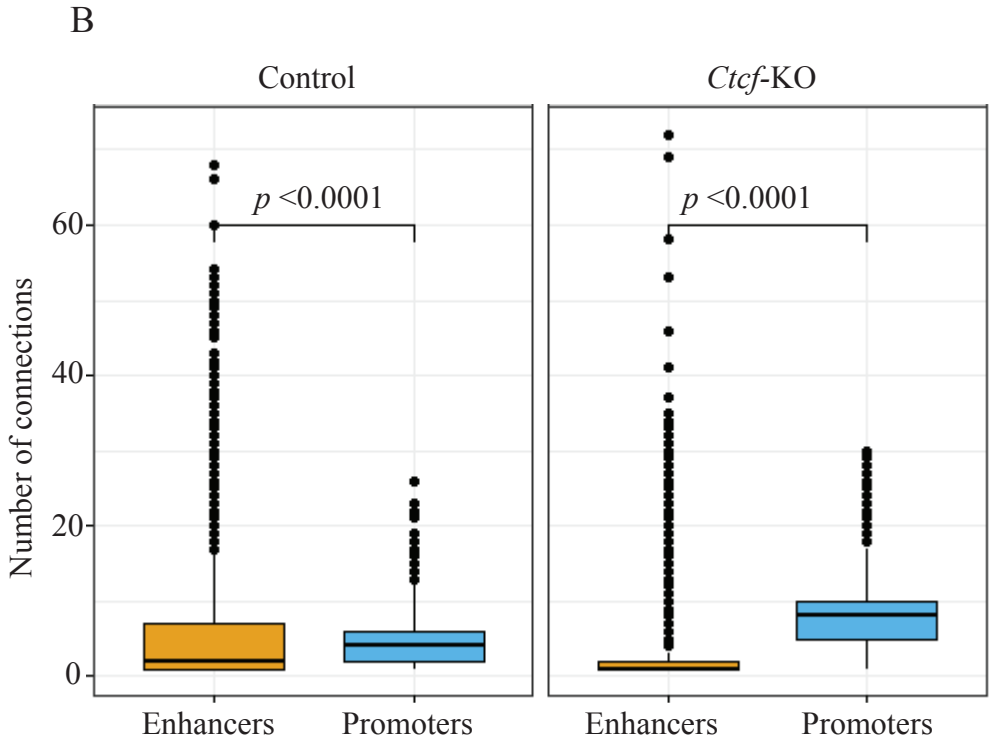

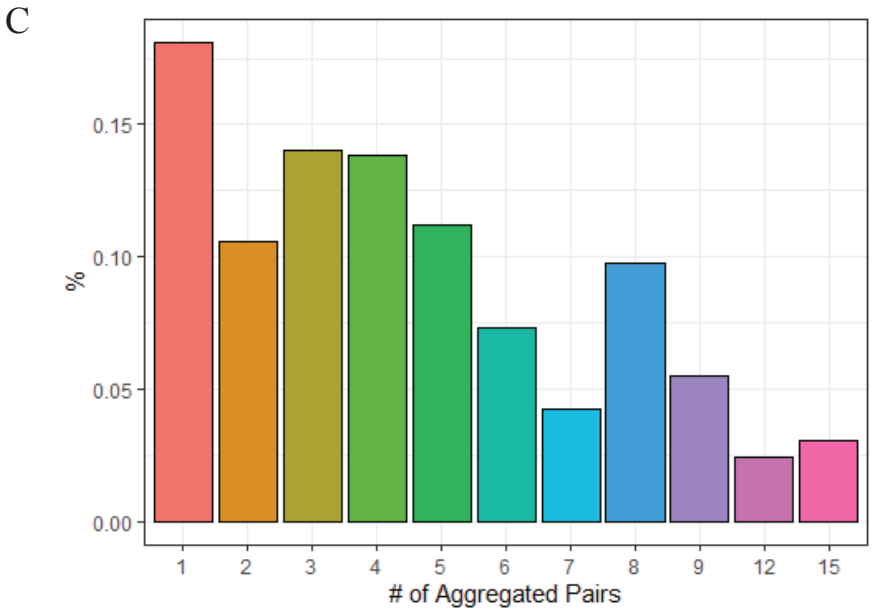

Supplementary Figure